Università di Pisa

Subthreshold behavior of dual-bit nonvolatile memories with very small regions of trapped charge

Luca Perniola
Dipartimento di Ingegneria dell'Informazione: Elettronica, Informatica, Telecomunicazioni,
Università di Pisa and IMEP-ENSERG, Grenoble
Giuseppe Iannaccone
Dipartimento di Ingegneria dell'Informazione: Elettronica, Informatica, Telecomunicazioni,
Università di Pisa
Gérard Ghibaudo
IMEP-ENSERG, Grenoble

L. Perniola, G. Iannaccone, G. Ghibaudo, *Subthreshold behavior of dual-bit nonvolatile memories with very small regions of trapped charge*, IEEE Trans. Nanotechnology, **5**, 4, pp.373-378 (2006).

Subthreshold Behavior of Dual-Bit Nonvolatile Memories With Very Small Regions of Trapped Charge

Luca Perniola, Giuseppe Iannaccone, and Gérard Ghibaudo

***Abstract*—We propose an analytical approach to investigate the electrostatic impact of very small charged regions in the gate dielectric of dual-bit nonvolatile memory cells based on discrete trapping sites, such as SONOS, NROM, or nanocrystal memories. Our model is based on the analytical solution of the Poisson equation for the surface potential in a fresh memory cell in subthreshold conditions. Then, we evaluate the effect of a small pocket of trapped charge on the surface potential using the superposition principle.**

Our proposed model is particularly accurate for small charged regions, down to the effective charged length $L_2 \simeq 10$ nm and for charge density up to $Q \simeq 10^{13}$ cm^{-2}. In addition, the proposed model represents a complementary approach to a previously developed model which was suitable for larger charged regions. Relevant consequences of the asymmetric charging of the storage layer on the electrical characteristics of discrete-trap memories are thoroughly analyzed. An analytical expression for the subthreshold slope factor S, the threshold voltage $V_{\rm th}$, and a method for extracting an "effective" distribution of charges from the transfer characteristics are derived.

***Index Terms*—Device modeling, discrete-trap memory, dual-bit, nanocrystal memory, nonvolatile memory, NROM, reverse read, second bit effect, SONOS.**

I. INTRODUCTION

NONUNIFORM injection in discrete-trap memories has recently attracted much attention in the literature for the possibility of encoding more than one bit for each memory cell. During the channel hot electron (CHE) stress, for instance, electrons are injected near the drain in the trapping medium, which can consist of an amorphous layer, as in NROM [2] and SONOS [3], or of a nanocrystal layer, as in nanocrystal flash memories [4], [5].

Nonuniform charging typically poses two issues: a difference between the threshold voltages extracted with forward ($V_{ds} > 0$) or reverse ($V_{ds} < 0$) read and a subthreshold slope degradation observed in reverse read [2], [4], [5].

Published studies on this subject are based on experiments or on two–dimensional (2-D) numerical simulations, in which much attention is devoted to the surface potential Ψ_S [6], [7]. One analytical approach, based on charge sharing, is able to provide an analytical approximated formula for the subthreshold slope S [8], and another analytical approach, based on the gradual channel approximation, is able to model the dual-bit performance in the triode operation region [9]. We have previously proposed an approach [1] based on the analytical calculation of the surface potential profile along the channel of a memory cell ideally consisting of a series of two MOSFETs, which is able to provide a reasonable solution in the limit of charged region larger than 20 nm.

The model we propose here is able to both extend the area of analysis to smaller regions and to provide an analytical formula for the subthreshold slope and the threshold voltage based on the surface potential approach. It starts from an analytical expression of the surface potential [1], [11] along the channel of a fresh cell and then it adds the effect of a charged region in the trapping medium close to the drain, via the superposition principle, provided that the memory cell is in a subthreshold region (where mobile charge is negligible with respect to space charge).

The main results of this new model are validated through a comparison with detailed numerical simulations performed with a 2-D TCAD package (ATLAS from SILVACO [10]).

II. ANALYTICAL MODEL FOR BULK MEMORY

A. Fresh Cell

The surface potential behavior along the channel can be computed as described in [11] and extended in [1] so that here we report only the results. The analytical solution to Ψ_S is a linear combination of hyperbolic sines

$$\Psi_S(y) = (\Psi_r - \Psi_L)\frac{\sinh(y/\lambda)}{\sinh(L/\lambda)} + (\Psi_l - \Psi_L)\frac{\sinh[(L-y)/\lambda]}{\sinh(L/\lambda)} + \Psi_L \quad (1)$$

where $y = 0$ ($y = L$) corresponds to the source (drain) contact, $\Psi_l = V_{bi} + V_s - V_b$, and $\Psi_r = V_{bi} + V_d - V_b$, where V_{bi} is the built-in voltage at the drain-bulk and source-bulk junctions, V_s is the source voltage, V_d is the drain voltage, V_b is the bulk voltage, and Ψ_L is the long channel surface potential [12]. The potential is set to zero in the bulk.

Manuscript received February 4, 2006; revised March 13, 2006. This work was supported in part by the EU under Projects ADAMANT (IST-2001-34234) and "SINANO" (IST-506844) and by the Italian CNR under the FIRB project "Sistemi miniaturizzati per elettronica e fotonica". The review of this paper was arranged by Associate Editor T. Hiramoto.

L. Perniola is with the CEA-LETI, 38054 Grenoble, France (e-mail: luca.perniola@cea.fr).

G. Iannaccone is with the Dipartimento di Ingegneria dell'Informazione, Universitàdegli Studi di Pisa, 56122 Pisa, Italy. He is also with the IEIIT-CNR, 56122 Pisa, Italy.

G. Ghibaudo is with the IMEP-CNRS/INPG, 38016 Grenoble, France.

Digital Object Identifier 10.1109/TNANO.2006.876920

1536-125X/$20.00 © 2006 IEEE

The parameter λ is defined as

$$\lambda \equiv \sqrt{\frac{\epsilon_{\rm si} t_{\rm eox} X_{\rm dep}}{\epsilon_{\rm ox}\eta}} \quad (2)$$

where $t_{\rm eox}$ is the equivalent oxide thickness, $X_{\rm dep}$ is the space charge region thickness, and $\epsilon_{\rm si(ox)}$ is the silicon (oxide) permittivity. Clearly, λ is a crucial parameter to describe short channel effects (SCEs), as it describes the influence of the pn junctions at the source and drain terminals on the behavior of Ψ_S. The higher the value of λ, the smoother the Ψ_S profile appears, and the weaker is the coupling between gate and channel. We stress that in this characteristic length we find the crucial parameters impacting on dual-bit performance. Moreover, λ is a function of η, which we obtain by fitting the surface potential behavior obtained from the numerical simulation with that obtained from the analytical model. Let us stress the fact that η is evaluated only once, for the fresh cell, and is valid for all charged configurations of the memory cell.

B. Electrostatic Effects of Trapped Charge

As a second step, the electrostatic effect of charges is considered via the superposition principle. As in [1], we assumed a uniform trapped charge region which is localized in the trapping layer next to the drain junction, while the region over the rest of the channel is free of charges. We believe that the simplified step-function distribution allows us to understand the programming behavior in terms of two effective parameters, an effective charged length L_2 and an effective charge density Q. When the overall channel is under weak inversion, the amount of mobile charge is so small that the Poisson equation can be considered linear. As shown in Fig. 1, in the 2-D structure the perturbative potential Ψ_{Sp}, due to a rectangular charged region of height t_{tm} and length L_2, is obtained by integrating the elementary contributions along the vertical direction x and longitudinal direction y [13]

$$\Psi_{Sp}^{(A)}(y) = \frac{-\rho}{\pi(\epsilon_{\rm si}+\epsilon_{\rm ox})} \times \int_{L_1}^{L_1+L_2} dy' \int_{t_1}^{t_1+t_{tm}} \ln\left(\sqrt{(y-y')^2+x^2}\right) dx \quad (3)$$

where ρ is the density of injected charge per unit volume and the apex A refers the integration to the actual pocket of charge, t_1 is the bottom oxide thickness and $L_1 = L - L_2$. Equation (3) has a closed-form solution. The boundary conditions of the Poisson equation are simplified as shown in Fig. 1 and can be taken into account by a proper configuration of image charges. The gate contact and the drain junction can be approximated as two perfect metals (one horizontal and one vertical plate, respectively), which enforce Dirichlet boundary conditions; therefore, the "real" charges must be suitably mirrored as indicated in Fig. 1. The Si/SiO_2 interface causes a change of permittivity from $\epsilon_{\rm si}$ to $\epsilon_{\rm ox}$ and this effect can be reproduced with basic electrostatic considerations [13], multiplying all the charges by a factor $\alpha = 2\epsilon_{\rm si}/(\epsilon_{\rm si}+\epsilon_{\rm ox})$.

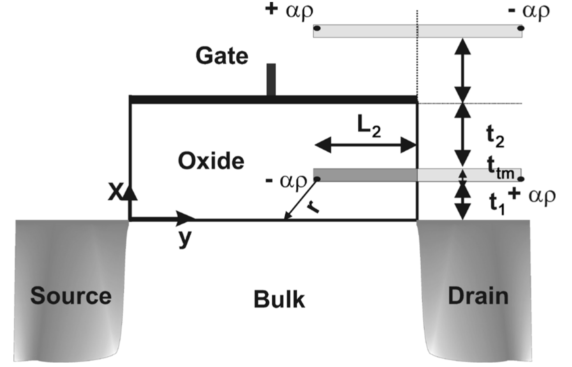

Fig. 1. Sketch of device to be considered for calculation of surface potential Ψ_{Stot}, where actual and image point charges are highlighted. Their impact on $\Psi_{\rm Stot}$ should be integrated along x and y of charged regions as indicated in (3). ρ stands for density of injected charge ($[\rho] = {\rm C/cm^3}$), and $\alpha = 2\epsilon_{\rm si}/(\epsilon_{\rm si}+\epsilon_{\rm ox})$ is multiplying factor due to presence of interface between two different materials (Si/SiO_2).

Each of the four pockets of charge shown in Fig. 1 provides a potential given by an integral equivalent to (3) with a closed-form solution. By summing up all four contributions, we obtain the perturbative potential Ψ_{Sp} and finally the surface potential $\Psi_{\rm Stot} = \Psi_S + \Psi_{Sp}$.

The current is calculated afterward as a diffusion dominated process [14], depending on the minimum of the surface potential $\Psi_{\rm Smin} = \min_y\{\Psi_{\rm Stot}\}$

$$I_{ds} = \frac{\mu_{\rm eff} W}{L_i}\sqrt{\frac{\epsilon_{\rm si} q N_{\rm sub}}{2(\Psi_{\rm Smin}+V_b)}}\left(\frac{KT}{q}\frac{n_i}{N_{\rm sub}}\right)^2 \times \exp\left[\frac{q(\Psi_{\rm Smin}+V_b)}{KT}\right] \quad (4)$$

where $\mu_{\rm eff}$ is the effective mobility of electrons in the channel, $N_{\rm sub}$ is the doping level of the bulk, T is the absolute temperature, q is the electron charge, n_i is the intrinsic electron concentration, and W is the cell width. The choice of L_i ($i = 1, 2$) depends on the region that includes the minimum of the surface potential $\Psi_{\rm Smin}$. If there is a complete punchthrough, $\Psi_{\rm Smin}$ stands under the uncharged region; thus, $L_i = L_1$. We stress that we numerically verify that (4) describes well the drain current in subthreshold region with reasonable error, for any value of L_2; moreover, due to the fact that the dual-bit behavior is usually sensed at high V_{ds} (i.e., $V_{ds} \simeq 1.5$ V), we neglected in (4) the effect of an applied drain voltage.

C. Domain of Validity of Analytical Model

We will perform the analysis for very low V_g, when the channel is in subthreshold or weakly inverted, where the linearity of the Poisson problem is retained. Approaching the inversion condition, such an assumption does not hold. However, provided that in the subthreshold region the drain current is exponential, the analytical transfer characteristic is obtained by extrapolating the exponential fit at low V_g (we extract the threshold voltage for $I_{ds} = 10$ nA).

For a very high density of charge ($Q \gtrsim 10^{13}$ cm^{-2}) and a very short charged region ($L_2 \lesssim 7$ nm), the error between

the analytical model predictions and the TCAD results becomes large (>15%). In such conditions, the model is no more applicable because of the occurrence of a punchthrough effect. From TCAD simulations, we have noticed that the maximum of the potential is far from the surface and the current flows at a certain distance from the interface; therefore, the model underestimates the drain current.

III. Analytical Expression of Subthreshold Slope Factor S and Threshold Voltage $V_{\rm th}$

Our analytical approach to the dual-bit behavior, in discrete trap memories, allows us to provide an analytical expression for the subthreshold slope factor S and the threshold voltage. Concerning S, the following reasoning is applied to the reverse reading, as the subthreshold slope degradation is visible for small values of L_2 and high Q only in reverse reading, while the forward reading shows the same characteristic of the fresh cell. The definition of the subthreshold slope factor S [14] is

$$S \equiv \frac{dV_g}{d(\log I_{ds})} = \frac{dV_g}{d\Psi_{\rm Smin}}\frac{d\Psi_{\rm Smin}}{d\log I_{ds}}. \quad (5)$$

We should properly evaluate the factor $dV_g/(d\Psi_{\rm Smin})$, and, to this aim, we need first to find the y_0 coordinate for which $d\Psi_{\rm Stot}(y)/dy = 0$. It is clear that in this way the derivation does not provide an explicit solution since the expression of $\Psi_{\rm Stot}(y)$ is not simple [see (1) and (3)]. A simpler way to obtain an approximated surface potential $\Psi^\star_{\rm Stot}$ is to perform a Taylor expansion of $\Psi_{\rm Stot}$ around the middle of the charged region ($\tilde{y} = L_1 + L_2/2$) close to the likely minimum of the function

$$\Psi^\star_{\rm Stot}(y) = \Psi_{\rm Stot}\big|_{y=\tilde{y}} + \frac{d\Psi_{\rm Stot}}{dy}\bigg|_{y=\tilde{y}} \cdot (y-\tilde{y}) + \frac{1}{2}\frac{d^2\Psi_{\rm Stot}}{dy^2}\bigg|_{y=\tilde{y}} \cdot (y-\tilde{y})^2. \quad (6)$$

Putting to zero the derivative of $\Psi^\star_{\rm Stot}$ with respect to y, we find the minimum y_0 and the minimum of the surface potential $\Psi^\star_{\rm Smin}$

$$y_0 = -\frac{d\Psi_{\rm Stot}/dy}{d^2\Psi_{\rm Stot}/dy^2} + \tilde{y}, \quad \Psi^\star_{\rm Smin} = \Psi^\star_{\rm Stot}(y_0). \quad (7)$$

Since Ψ_{Sp} does not depend on V_g, in the end, we can write the following analytical formula:

$$\frac{d\Psi^*_{\rm Smin}}{dV_g} = \frac{d\Psi_S}{dV_g} + \frac{d^2\Psi_S}{dydV_g}\cdot\Delta\tilde{y} \quad (8)$$

where $\Delta\tilde{y} \equiv y_0 - \tilde{y}$ and all terms on the right-hand side are calculated in $y = \tilde{y}$ and $V_g = V_{fb} + \phi_F + \gamma\sqrt{\phi_F}$, i.e., weak inversion ($V_{fb}$ is the flat band voltage, γ the body factor, and ϕ_F the bulk Fermi level). A third-order term in (8) would only slightly improve the overall precision and therefore is neglected.

The terms of (8) are

$$\begin{aligned}
&\frac{d\Psi_S}{dV_g} = \left[1 - \frac{\sinh\left(\frac{\tilde{y}}{\lambda}\right) + \sinh\left(\frac{L-\tilde{y}}{\lambda}\right)}{\sinh\left(\frac{L}{\lambda}\right)}\right] \times \left[1 - \frac{\gamma}{\sqrt{\gamma^2 + 4(2\phi_F + \gamma\sqrt{2\phi_F})}}\right]^{-1}\\
&\frac{d^2\Psi_S}{dydV_g} = \frac{\cosh\left(\frac{L-\tilde{y}}{\lambda}\right) - \cosh\left(\frac{\tilde{y}}{\lambda}\right)}{\lambda\sinh\left(\frac{L}{\lambda}\right)} \times \left[1 - \frac{\gamma}{\sqrt{\gamma^2 + 4(2\phi_F + \gamma\sqrt{2\phi_F})}}\right]^{-1}\\
&\frac{d\Psi_S}{dy} = (\Psi_r - \Psi_L)\frac{\cosh\left(\frac{\tilde{y}}{\lambda}\right)}{\lambda\sinh\left(\frac{L}{\lambda}\right)} - (\Psi_l - \Psi_L)\frac{\cosh\left(\frac{L-\tilde{y}}{\lambda}\right)}{\lambda\sinh\left(\frac{L}{\lambda}\right)}\\
&\frac{d^2\Psi_S}{dy^2} = (\Psi_r - \Psi_L)\frac{\sinh\left(\frac{\tilde{y}}{\lambda}\right)}{\lambda^2\sinh\left(\frac{L}{\lambda}\right)} + (\Psi_l - \Psi_L)\frac{\sinh\left(\frac{L-\tilde{y}}{\lambda}\right)}{\lambda^2\sinh\left(\frac{L}{\lambda}\right)}\\
&\frac{d\Psi_{Sp}}{dy} = \frac{\rho q}{\pi\epsilon_{\rm ox}}\left[\psi'_{Sp}(t_1+t_{tm}, t_1) - \psi'_{Sp}(t_{\rm eox}+t_{tm}+t_2, t_{\rm eox}+t_2)\right]\\
&\psi'_{Sp}(R,M) = \frac{R}{2}\ln\left\{\frac{\left[R^2+(L_1-\tilde{y})^2\right]\left[R^2+(L_1+2L_2-\tilde{y})^2\right]}{\left[R^2+(L-\tilde{y})^2\right]^2}\right\}\\
&\quad + \frac{M}{2}\ln\left\{\frac{\left[M^2+(L-\tilde{y})^2\right]^2}{\left[M^2+(L_1-\tilde{y})^2\right]\left[M^2+(L_1+2L_2-\tilde{y})^2\right]}\right\}\\
&\quad + (L_1-\tilde{y})\left[\arctan\left(\frac{t_{tm}(L_1-\tilde{y})}{(L_1-\tilde{y})^2+R\cdot M}\right)\right]\\
&\quad + (L_1+2L_2-\tilde{y})\left[\arctan\left(\frac{t_{tm}(L_1+2L_2-\tilde{y})}{(L_1+2L_2-\tilde{y})^2+R\cdot M}\right)\right]\\
&\quad - 2(L-\tilde{y})\left[\arctan\left(\frac{t_{tm}(L-\tilde{y})}{(L-\tilde{y})^2+R\cdot M}\right)\right]\\
&\frac{d^2\Psi_{Sp}}{dy^2} = \frac{\rho q}{\pi\epsilon_{\rm ox}}\left[\psi''_{Sp}(t_1+t_{tm}, t_1) - \psi''_{Sp}(t_{\rm eox}+t_{tm}+t_2, t_{\rm eox}+t_2)\right]\\
&\psi''_{Sp}(R,M) = \arctan\left[\frac{(L-\tilde{y})t_{tm}}{(L-\tilde{y})^2+R\cdot M}\right] - \arctan\left[\frac{(L_1-\tilde{y})t_{tm}}{(L_1-\tilde{y})^2+R\cdot M}\right]\\
&\quad - \arctan\left[\frac{(L_1+2L_2-\tilde{y})t_{tm}}{(L_1+2L_2-\tilde{y})^2+R\cdot M}\right].
\end{aligned} \quad (9)$$

The threshold voltage $V_{\rm th}$ is the V_g corresponding to a given I_{ds}. We have to analytically find the behavior of V_g as a function of $\Psi^\star_{\rm Smin}$, which comes from the inversion of (6). Stressing the fact that in (6) the minimum y_0 is only slightly dependent on V_g, we consider it constant at the value of $V_g \equiv V_{\rm th-L} = V_{fb} + 2\phi_F + \gamma\sqrt{2\phi_F}$ (i.e., at the onset of inversion). Then, the only dependence on V_g in (1), (6), and (7) resides in the long channel surface potential, developed around $\Psi_L = 2\phi_F$

$$\Psi_L = \frac{V_g - V_{\rm th-L}}{1 + \frac{\gamma}{\sqrt{8\phi_F}}} + 2\phi_F. \tag{10}$$

By inverting (6), we therefore obtain

$$V_{\rm th} = \left(-\frac{\Psi^\star_{\rm Smin}(I_{ds}) - K}{H} - 2\phi_F\right)\left(1 + \frac{\gamma}{\sqrt{8\phi_F}}\right) + V_{\rm th-L} \tag{11}$$

where

$$K = \left[\psi_r \frac{\sinh(\tilde{y}/\lambda)}{\sinh(L/\lambda)} + \psi_l \frac{\sinh\left(\frac{L-\tilde{y}}{\lambda}\right)}{\sinh(L/\lambda)}\right] \times \left(1 + \frac{\Delta\tilde{y}}{\lambda}\right) + \Psi_{Sp} + \frac{d\Psi_{Sp}}{dx}\Delta\tilde{y}$$

$$H = \frac{\sinh(\tilde{y}/\lambda)}{\sinh(L/\lambda)} + \frac{\sinh\left(\frac{L-\tilde{y}}{\lambda}\right)}{\sinh(L/\lambda)} - 1 + \frac{\Delta\tilde{y}}{\lambda}\left[\frac{\cosh(\tilde{y}/\lambda) - \cosh\left(\frac{L-\tilde{y}}{\lambda}\right)}{\sinh(L/\lambda)}\right]$$

where in K, the Ψ_{Sp} contributions obviously exist only if we calculate the threshold voltage of a charged cell. $\Psi^\star_{\rm Smin}(I_{ds})$ comes from the inversion of (4) and depends on the drain current at which the threshold voltage is calculated.

In the development of (8)–(11), we assumed that the minimum y_0 (7) resides under the charged region L_2. If this region is so small that y_0 resides under L_1, the Taylor expansion of $\Psi_{\rm Stot}$ should be made around the middle of the cell, and the previously mentioned formulas are still valid with $\tilde{y} = L/2$. Indeed, we note that in Fig. 2, if $L_2 \lesssim 15$ nm, the subthreshold slope regains the fresh cell solution and the threshold voltage shift becomes zero.

IV. Numerical and Analytical Results

In order to assess the viability of this model, the 2-D numerical TCAD tool ATLAS has been used [10]. The device under investigation is an idealized typical NROM device. The width and length of the cell are 0.16 and 0.28 μm, respectively, drain and source n-doping is at $N_d = 10^{19}$ cm^{-3}, the p-channel doping is $N_{\rm sub} = 5 \times 10^{17}$ cm^{-3}, the bottom oxide thickness is $t_1 = 7$ nm, and the top oxide thickness is $t_2 = 9$ nm. Concerning the trapping layer, for the sake of simplicity, we have considered an SiO_2 layer $t_{tm} = 3.6$ nm, equivalent, from an electrostatic point of view, to a layer of silicon nitride of 7 nm. We have verified that even in the case of nonuniform charging, the substitution of the silicon nitride layer with an equivalent silicon oxide layer has a negligible effect on the results of the simulation. In the following discussion, the threshold voltage is taken at $I_{ds} = 10$ nA.

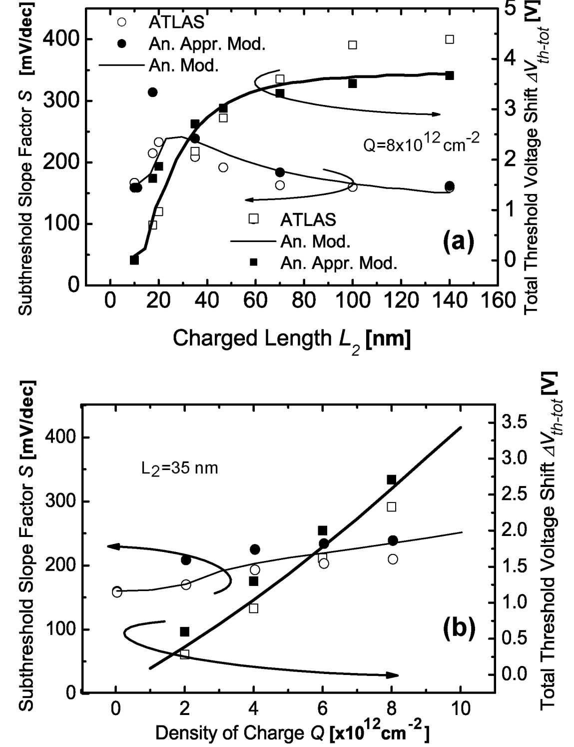

Fig. 2. Comparison between TCAD results, results from analytical model [eqs. (1)–(3)] and from approximated model (eq. (6)–(8)) concerning total threshold voltage shift $\Delta V_{\rm th-tot}$ and subthreshold slope S factor. (a) Range of values for charged length is 7 nm $\leq L_2 \leq$ 140 nm, density of charge is fixed at $Q = 8 \times 10^{12}$ cm^{-2}. As is intuitive, in raising value of charged length, $\Delta V_{\rm th-tot}$ raises as well. Instead, subthreshold slope S exhibits maximum. (b) Range of values for density of charge is 10^{12} cm^{-2} $\leq Q \leq 10^{13}$ cm^{-2}, charged length is fixed at $L_2 = 35$ nm. We notice that $\Delta V_{\rm th-tot}$ and S raise monotonically, if density of charge gets larger and larger.

In Fig. 2, we show the comparison between TCAD and analytical results, concerning the subthreshold slope factor S and the total threshold voltage shift $\Delta V_{\rm th-tot}$, for different values of L_2 and Q. In Fig. 2(a), we note that for very small values of L_2, S is close to that of a fresh cell, while by raising the value of L_2 the subthreshold slope degrades up to a maximum value ($\sim L_2 \simeq 30$ nm); then, S goes again to the smaller fresh cell limit as the portion of the charged cell approaches the overall length. On the other hand, in Fig. 2(b) we note that, by raising the value of Q, the subthreshold slope keeps degrading. A similar behavior of the subthreshold slope factor has been previously shown in [8].

V. Contour Plot of $\Delta V_{\rm th-tot}$ and S With Respect to L_2 and Q

In the previous section, the behavior of the forward read transfer characteristics has not been mentioned. Such an issue has been addressed in our previous approach [1], and, given that the present model is tailored specifically for very short charged length L_2, the forward read would provide an $I_D - V_{GS}$ curve basically identical to that of a fresh cell. If we consider a large

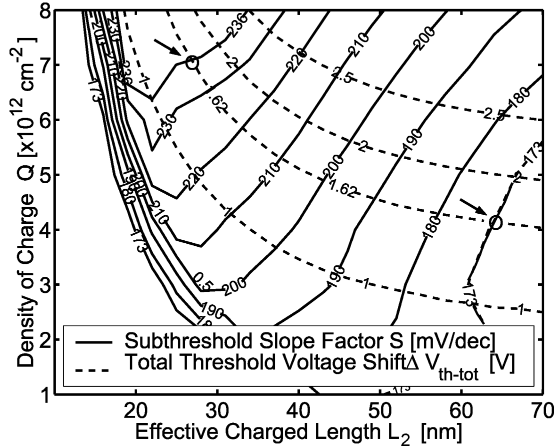

Fig. 3. Contour plots of $\Delta V_{\rm th-tot}$ (dashed line) and S (solid line) as function of L_2 and Q for $|V_{ds}| = 1.5$ V. From experimental data, we find cross point between $\Delta V_{\rm th-tot}$ and S values, and we are able to extract information on charge distribution injected in trapping medium through L_2 and Q. Two sample crosses for $I_D - V_{GS}$ are shown in Fig. 4.

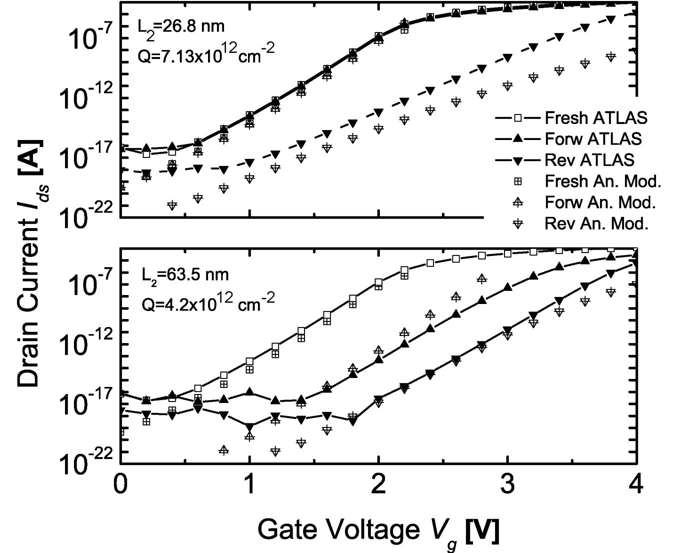

Fig. 4. Check of viability of analytical model. Two cross points are chosen from map: $\Delta V_{\rm th-tot} = 1.6$ V in both cases, while $S = 176$ mV/dec and $S = 233$ mV/dec. According to contour plots of Fig. 3, $Q = 4.2 \times 10^{12}$ cm^{-2}, $L_2 = 63.5$ nm, $Q = 7.13 \times 10^{12}$ cm^{-2}, and $L_2 = 26.85$ nm are deduced. Values are used in ATLAS input deck and numerical $I_D - V_{GS}$ characteristics are plotted. Reasonable agreement between data and numerical simulation is found, which means that L_2 and Q from analytical model are rather reliable.

L_2 ($L_2 \gtrsim 70$ nm), the forward read follows the behavior shown in [1], but, in that range of L_2, the subthreshold slope (forward or reverse read) is similar to that of a fresh cell as shown already in Fig. 2.

With the help of this model, we can concentrate, indeed, on the behavior of the subthreshold slope and on the behavior of the total threshold voltage shift, focusing on the transfer characteristics of the fresh cell and of the written cell in the reverse read.

In Fig. 3, we provide two contour plots of $\Delta V_{\rm th-tot}$ and S, with respect to L_2 and Q. From the experiments, we can have information on the threshold voltage in the fresh read ($V_{\rm th-fresh}$), reverse read ($V_{\rm th-R}$), and the value of the subthreshold slope factor S. We identify one cross point on the map of Fig. 3 and we deduce the features of the effective charge distribution trapped near the drain, L_2 and Q.

We stress the fact that we can use this model to get other contour plots of the programming windows, not only of $\Delta V_{\rm th-tot}$ and S, depending of the information that we have at hand from experiments, and extract the two features of the pocket of charge.

These kinds of contour plots are interesting in the sense that they provide a simple information on the actual state of the pocket of injected charge. For instance, they can be used also during data retention experiments to understand whether the diffusion process among traps, i.e., $Q \times L_2 = {\rm const.}$, or the charge leakage towards the channel, i.e., $L_2 = {\rm const.}$, is the predominant effect affecting data retention: a clear different electrical behavior would be visible in these contour plots function of Q and L_2 [15].

Just as a check of the validity of such a map, we compare results from our model with numerical simulations. We extract from the map Q and L_2, for a pair of $\Delta V_{\rm th-tot}$ and S, and use them in the 2-D TCAD simulator to see if simulated electrical characteristics are in agreement with the given values of $\Delta V_{\rm th-tot}$ and S. The results of such a comparison for two typical cases are shown in Fig. 4 where, according to the contour plots, $\Delta V_{\rm th-tot} = 1.62$ V in both cases and $S = 173$ mV/dec or $S = 236$ mV/dec; the reasonable agreement obtained shows that the proposed maps are useful to extract an "effective" distribution of the trapped charge.

VI. Conclusion

We have presented an analytical model that provides a simple electrostatic view of dual-bit memory electrical behavior. The reverse mode read and forward mode read of a programmed cell with nonuniform distribution of injected charge are analytically computed. The main issues such as the higher threshold voltage in reverse read than in forward read and the subthreshold slope degradation in reverse read are all successfully addressed. In particular, the subthreshold slope degradation is caused by a very small pocket of charge ($L_2 \lesssim 30$ nm) with very high density of charge ($Q \gtrsim 10^{12}$ cm^{-2}). The overall reasoning needs only one physically based η parameter, which depends on the features of the fresh cell and is completely independent of the effective distribution of the pocket of charge. The proposed model pushes the limits of the analysis to a distribution of charges with $L_2 \simeq 10$ nm and $Q \simeq 10^{13}$ cm^{-2}.

With the help of this model we are able to extract the features of the injected pocket of charge from simple contour plots as provided in Fig. 3. Moreover, an analytical approximated formula for the subthreshold slope factor and the threshold voltage are provided. We consider this model an effective tool for the comprehension of dual-bit memory behavior of nonvolatile memories such as SONOS, NROM, or nanocrystal.

Acknowledgment

The authors would like to thank B. De Salvo, from CEA/LETI (Grenoble, France), for helpful discussions on the technological issues of the nanocrystal memory cell. They would also like to

thank G. Mugnaini, from the University of Pisa, Pisa, Italy, for the support on modeling aspects of the subject.

REFERENCES

[1] L. Perniola, S. Bernardini, G. Iannaccone, P. Masson, B. De Salvo, G. Ghibaudo, and C. Gerardi, "Analytical model of the effects of a non-uniform distribution of stored charge on the electrical characteristics of discrete-trap non-volatile memories," *IEEE Trans. Nanotech.*, vol. 4, no. 3, pp. 360–368, May 2005.

[2] B. Eitan, P. Pavan, I. Bloom, E. Aloni, A. Frommer, and D. Finzi, "NROM: A novel localized trapping, 2-bit nonvolatile memory cell," *IEEE Electron Device Lett.*, vol. 21, no. 11, pp. 543–545, Nov. 2000.

[3] C. T. Swift, G. L. Chindalore, K. Harber, T. S. Harp, A. Hoefler, C. M. Hong, P. A. Ingersoll, C. B. Li, E. J. Prinz, and J. A. Yater, "An embedded 90 nm SONOS nonvolatile memory utilizing hot electron programming and uniform tunnel erase," in *Int. Electron Device Meeting (IEDM) Tech. Dig.*, 2002, pp. 927–930.

[4] B. De Salvo *et al.*, "How far will silicon nanocrystals push the scaling limits of NVMs technologies?," in *Int. Electron Device Meeting (IEDM) Tech. Dig.*, 2003, pp. 597–600.

[5] R. Muralidhar *et al.*, "A 6 V embedded 90 nm silicon nanocrystal nonvolatile memory," in *Int. Electron Device Meeting (IEDM) Tech. Dig.*, 2003, pp. 601–604.

[6] E. Lusky, Y. S. Diamand, I. Bloom, and B. Eitan, "Characterization of channel hot electron injection by the subthreshold slope of NROM device," *IEEE Electron Device Lett.*, vol. 22, no. 11, pp. 556–558, Nov. 2001.

[7] M. Sadd *et al.*, "A model for the channel potential of charge-trapping memories and its implications for device scaling," *Solid State El.*, vol. 49, pp. 1754–1758, 2005.

[8] A. Shappir, Y. S. Diamand, E. Lusky, I. Bloom, and B. Eitan, "Subthreshold slope degradation model for localized-charge-trapping based non-volatile memory devices," *Solid State El.*, vol. 47, pp. 937–941, 2003.

[9] Y. W. Chang, T. C. Lu, S. Pam, and C. Y. Lu, "Modeling for the 2nd-bit effect of a nitride-based trapping storage flash EEPROM cell under two-bit operation," *IEEE Electron Device Lett.*, vol. 25, no. 2, Feb. 2004.

[10] SILVACO-ATLAS User's Manual vol. I–II.

[11] Z. H. Liu, C. Hu, J. H. Huang, T. Y. Chan, M. C. Jeng, P. K. Ko, and Y. C. Cheng, "Threshold voltage model for deep-submicrometer MOSFET's," *IEEE Trans. Electron Devices*, vol. 40, no. 1, pp. 86–95, Jan. 1993.

[12] Y. Tsividis, *Operation and Modeling of the MOS Transistor*, 2nd ed. New York: Columbia Univ., 1999, p. 74.

[13] L. D. Landau, E. M. Lifshitz, and L. P. Pitaevskii, *Electrodynamics of Continuous Media*, 2nd ed. London, U.K.: Butterworth-Heinemann, 1984.

[14] Y. Taur and T. H. Ning, *Fundamentals of Modern VLSI Devices*. Cambridge, U.K.: Cambridge. Univ. Press, 1998, p. 128.

[15] L. Perniola *et al.*, "Experimental and theoretical analysis of scaling issues in dual-bit discrete trap nonvolatile memories," in *Int. Electron Device Meeting (IEDM) Tech. Dig. 2005*, pp. 857–860.

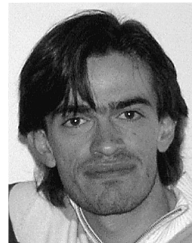

Luca Perniola was born in 1978 in Florence, Italy. He received the Laurea degree in nuclear engineering from the Politecnico di Milano, Milan, Italy, in 2002, and the Ph. D. degree from the University of Pisa, Pisa, Italy, and the Institut National Polytechnique de Grenoble, Grenoble, France, in 2005, with a thesis on modeling and electrical characterization of discrete-trap nonvolatile memory devices.

He has recently joined the modeling and electrical characterization group of microelectronic devices (LSCDP) of CEA-LETI, Grenoble. His research interests include the modeling of electrical properties of memory devices with discrete storage nodes in planar and more complex structures (i.e., FinFET).

Giuseppe Iannaccone was born on April 28, 1968. He received the Laurea degree in electrical engineering and the Ph.D. degree the University of Pisa, Pisa, Italy, in 1992 and 1996, respectively.

In 1996, he took a permanent position as a Researcher with the Italian National Research Council, and in the same year he obtained a faculty position at the Electrical Engineering Deparment, University of Pisa, first as an Assistant Professor, then, since January 2001, as an Associate Professor. His research interests include transport and noise modeling in nanoelectronic devices, development of TCAD tools, the investigation of limits to scaling down of CMOS technology, and the exploitation of nanoscale effects in alternative devices structures. More recently, he has been active in the design of extremely low power systems for RFID and ambient intelligence scenarios. He has been a Principal Investigator for a few national and European projects. He is the author of more than 90 papers published in peer reviewed journals and more than 60 papers in the proceedings of international conferences.

Gérard Ghibaudo was born in France, in 1954. He graduated, in 1979, received the Ph.D. degree in electronics, in 1981, and the State Thesis degree in physics, in 1984, all from the Polytechnics Institute of Grenoble, Grenoble, France.

He became an Associate Researcher at CNRS, Grenoble, in 1981, where he is now Director of Research at Laboratories of Semiconductor devices (LPCS/ENSERG now IMEP/ENSERG). During the academic year 1987 to 1988, he spent a sabbatical year at the Naval Research Laboratory, Washington, DC, where he worked on the characterization of MOSFETs. His research activities include the field of electronics transport, oxidation of silicon, MOS device physics, fluctuations, and lo— frequency noise and dielectric reliability. During his career, he has been author or coauthor of over 210 articles in international refereed journals, 330 communications, and 35 invited presentations in international conferences as well as 12 book chapters.

Dr. G. Ghibaudo was or is a member of several technical/scientific committees of international conferences (ESSDERC 93&99&03, WOLTE, ICMTS, MIEL 95-2004, ESREF 96-98-00-03-04-05, SISC, MIGAS, ULIS, IEEE/IPFA, . . .). He was Cofounder of the First European Workshop on Low Temperature Electronics (WOLTE 94) and Organizer of eight Workshops/Summer School during the last ten years. He is also a member of the editorial board of *Solid State Electronics* and *Microelectronics Reliability*.